Design Trade-Offs Between the Coupled Coils' Inductance and the Series-Series Compensation Capacitance for EV Wireless Charging Systems

Grazian, Francesca; Soeiro, Thiago Batista; Bauer, Pavol

DOI
10.1109/SPEEDAM53979.2022.9842278

Publication date
2022

Document Version
Accepted author manuscript

Published in
Proceedings of the 2022 International Symposium on Power Electronics, Electrical Drives, Automation and Motion (SPEEDAM)

Design Trade-Offs Between the Coupled Coils' Inductance and the Series-Series Compensation Capacitance for EV Wireless Charging Systems

Francesca Grazian, Thiago Batista Soeiro and Pavol Bauer
Delft University of Technology
Delft, The Netherlands
Email: (F.Grazian, T.BatistaSoeiro, P.Bauer)@tudelft.nl

***Abstract*—Nowadays, inductive power transfer (IPT) with magnetic resonance is the most used method for high-power wireless battery charging applications. Once the topology of the compensation network and the operating frequency are selected, there are infinite combinations of the circuit equivalent inductance and compensation capacitance values resonating at that frequency. Choosing an appropriate ratio between these passive devices is essential to meet the target output power while ensuring that the required DC input and output voltages are found within the permitted range limited by the power source and the battery load. This paper proposes design trade-offs for selecting the optimum ratio between the inductance and capacitance in IPT systems with series-series compensation applicable to any power level. First, the target mutual inductance must be computed. Based on that, the coupled coils are designed depending on the physical constraints. An example is provided considering a 3.7 kW wireless charging system for electric vehicles (EVs) where different coils' combinations are analyzed through the finite element method. The most suitable design is implemented, achieving or the application a relatively high measured peak DC-to-DC efficiency of about 96.24% at 3.28kW while the coils are aligned with 11cm distance. The required power is delivered at different battery voltages and coils' alignments by regulating the DC input voltage.**

***Index Terms*—Electric vehicles, inductive power transfer, series-series compensation network, wireless charging.**

I. Introduction

In the last decade, wireless charging has gained increasing interest in the field of battery charging for implanted medical devices, consumer electronics, and electric vehicles (EVs) [1]. In relatively high-power applications, inductive power transfer (IPT) with magnetic resonance is mostly used [2]. This method works through coupled coils that exchange power via a high-frequency magnetic field. In order to reach a high power transfer, this frequency is tuned by the power electronic converter switches to form a resonating link between the coupled coils' inductance and added compensation capacitance.

Suppose a single capacitor is connected to each coil. In that case, there are four possible resonant-based power converters according to whether the connection is placed in series or parallel with the main coupled coils. These basic compensations networks are called series-series (S-S), series-parallel (S-P), parallel-series (P-S), and parallel-parallel (P-P) [3], [4]. The S-S compensation is widely used since its capacitance value is independent of the coil's mutual inductance and the load. Moreover, the output of the S-S compensation has a current-source behavior that makes it suitable for the charging batteries since they are modeled as voltage sources. However, the S-S compensation is not inherently safe when the coils' alignment varies in a wide range, e.g., in dynamic charging of EVs, because the output current is inversely proportional to the coils' mutual inductance. This means that the output power increases with the coils' misalignment. In those cases, it is preferable to use compensation networks with multiple passive components because the output current is directly proportional to the coils' mutual inductance. The most known examples are the LCL and LCC compensations [5]–[7].

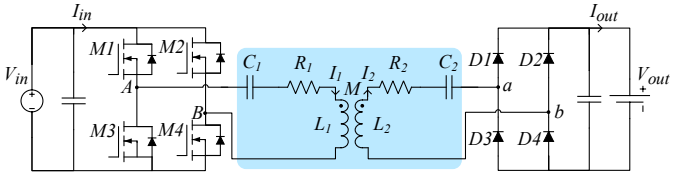

Fig. 1. Typical equivalent circuit of a IPT system for wireless charging of EVs that employes the S-S compensation network.

In the case of static EV wireless charging, the S-S compensation is generally preferred since the resonant circuit has the minimum number of passive components, and the coils' misalignment typically happens in a limited range. The analytical modeling of the S-S compensation has been well-exploited in [3], [4], [8]–[11]. However, while designing a certain wireless charging system, there are infinite combinations of coils' inductance and compensation capacitance values that resonate at a specific frequency. It is not always clear to engineers, designers and researches how to choose the values of these passive components. Nevertheless, it is fundamental to perform that selection process before designing and implementing the coupled coils and the compensation capacitors. The failure of this process could result in an EV wireless charging system with an unnecessary lower power transfer efficiency, a poor utilization of the DC-link input voltage, or possibly the loss of the H-bride inverter's soft-switching.

Specifically, the choice of the circuit parameters must result from several considerations. First, the desired power transfer level must be met at the chosen operating frequency range. Moreover, from the power electronics point of view, the DC input and output voltages must be within the allowed range defined by the power source, the load, and the implemented converter circuit components. The use of additional non-

isolated DC/DC converters cascaded to the basic resonant converter allows the extension of the input or output voltage range to fulfill the application's power transfer requirements. However, the voltage range of these converters is also limited, and it is preferable to use as few conversion stages as possible to guarantee low power losses and avoid additional manufacturing costs. Additionally, the current flowing through the switches must be kept low, and soft-switching must be ensured to limit the power losses in the converters' switches. From the resonant circuit's point of view, the voltage and current stress must be reasonable to reduce component cost, limit losses, and to simplify the manufacturing. The most favorable ratio between coils' inductance and compensation capacitance needs to satisfy all these requirements.

This paper proposes design trade-offs to optimize the selection of coils' inductance and compensation capacitance for S-S compensated EV wireless charging systems, which circuit schematic is shown in Fig. 1. The generalized methodology applicable to any power level is discussed in Section II. An example is proposed in Section III on a 3.7 kW system, of which coils' parameters are found through the finite element method (FEM) in COMSOL Multiphysics. The trade-off design is selected and implemented in a laboratory prototype achieving for the application at hand a relatively high measured peak DC-to-DC efficiency of 96.24%. Finally, the main conclusions are listed in Section IV.

II. Generalized Design Methodology

A. Analytical modeling of the S-S compensated circuit

The behavior in the frequency domain of the S-S compensation network in Fig. 1 is described by (1). Thereby, L_1 is the primary coil self-inductance and L_2 is the coil secondary self-inductance of which the magnetic coupling k depends on the coils' mutual inductance M as stated in (2). Moreover, C_1 and C_2 are the S-S compensation network's capacitances, and R_1 and R_2 are the lumped series resistances modeling the losses of the primary and the secondary circuits' components. The primary and secondary circuits' impedance $\boldsymbol{Z}_1$, $\boldsymbol{Z}_2$ are defined in (3). According to [12], the input voltage $\boldsymbol{V}_{AB}$ and the equivalent resisitive load R_{ac} are defined in (4).

$$\begin{cases} \boldsymbol{V}_{AB} = \boldsymbol{Z}_1\boldsymbol{I}_1 + j\omega M\boldsymbol{I}_2 \\ 0 = (\boldsymbol{Z}_2 + R_{ac})\boldsymbol{I}_2 + j\omega M\boldsymbol{I}_1 \end{cases} \tag{1}$$

$$M = k\sqrt{L_1 L_2} \tag{2}$$

$$\boldsymbol{Z}_i = R_i + j\omega X_i, \quad X_i = \omega L_i - \frac{1}{\omega C_i}: \quad i = 1...2 \tag{3}$$

$$\boldsymbol{V}_{AB} = V_{AB,1}\angle 0° = \frac{4}{\pi}V_{in}, \quad R_{ac} = \frac{8}{\pi^2}R_L = \frac{8}{\pi^2}\frac{V_{out}^2}{P_{out}} \tag{4}$$

B. Selection of the target mutual inductance

In the design of an IPT system, generally the chosen battery charging application defines the desired power level P_{out}, the nominal battery voltage V_{out} and its charging range, the available range of input voltage V_{in} from the power source, and the allowed resonant frequency range f_0=$\frac{\omega_0}{2\pi}$. After the identification of these inputs, it is possible to compute the approximate required M which results in (5). The latter has been calculated from (1)-(4), assuming: X_1=X_2=R_1=R_2=0.

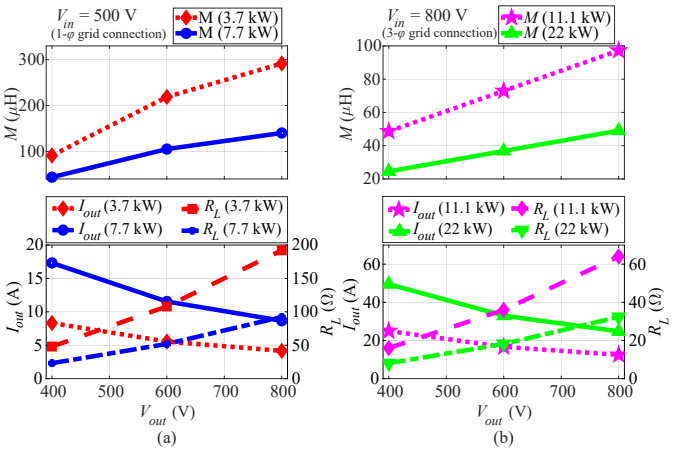

Fig. 2. Required mutual inductance M, DC output current I_{out}, and equivalent resistive load R_L depending on the nominal battery voltage V_{out} for the power levels P_{in} of: (a) 3.7 kW (WPT1), 7.7 kW (WPT2), and (b) 11.1 kW (WPT3), 22 kW (WPT4), where P_{out}=0.9·P_{in} and f_0 = 85 kHz.

When considering the application of EVs, SAE J2954 [13] regulates three power classes, namely WPT1, WPT2 and WPT3, which correspond to a maximum input power from the AC-grid of (3.3, 7.7, 11.1)kVA, respectively. The guidelines for 22kVA (WPT4 power class) are still under consideration [14]. Moreover, SAE J2954 defines the operating frequency range for the H-bridge inverter in Fig. 1, being 79...90 kHz.

$$M = \frac{8}{\pi^2}\frac{V_{in}V_{out}}{\omega_0 P_{out}} \tag{5}$$

From (5), it is intuitive that, for the same V_{in}, V_{out} and ω_0, each power level requires a different value of M. An example of that is shown in Fig. 2. Thereby, the power classes WPT1 and WPT2 have a single-phase (1-ϕ) connection to the European low-voltage 50 Hz grid, while a 3-ϕ grid connection is considered for WPT3 and WPT4. This choice is due of the fact that households in Europe have limited access to grid connections with more than 16 A for each 230 V phase.

Fig. 2 shows that the constraints imposed to a specific EV wireless charging application result in a required M that might differ considerably from other applications with different battery voltage or power class. For instance, considering all the uses cases in Fig. 2, the required M can be in the range 20...300 μH. If the coils' implementation does not result in the target M, the use of additional non-isolated DC/DC converters cascaded to the basic resonant converter allows the extension of the input or output voltage range to fulfill (5). However, this is not preferable to limit the power losses and avoid extra manufacturing costs.

C. Selection of the coils' and compensation's parameters

After the identification of the target M, it is now important to choose the combination of inductance and capacitance that leads to a high efficiency operation. The selection of the coils' parameters L_1, R_1, L_2, R_2 and k is performed through

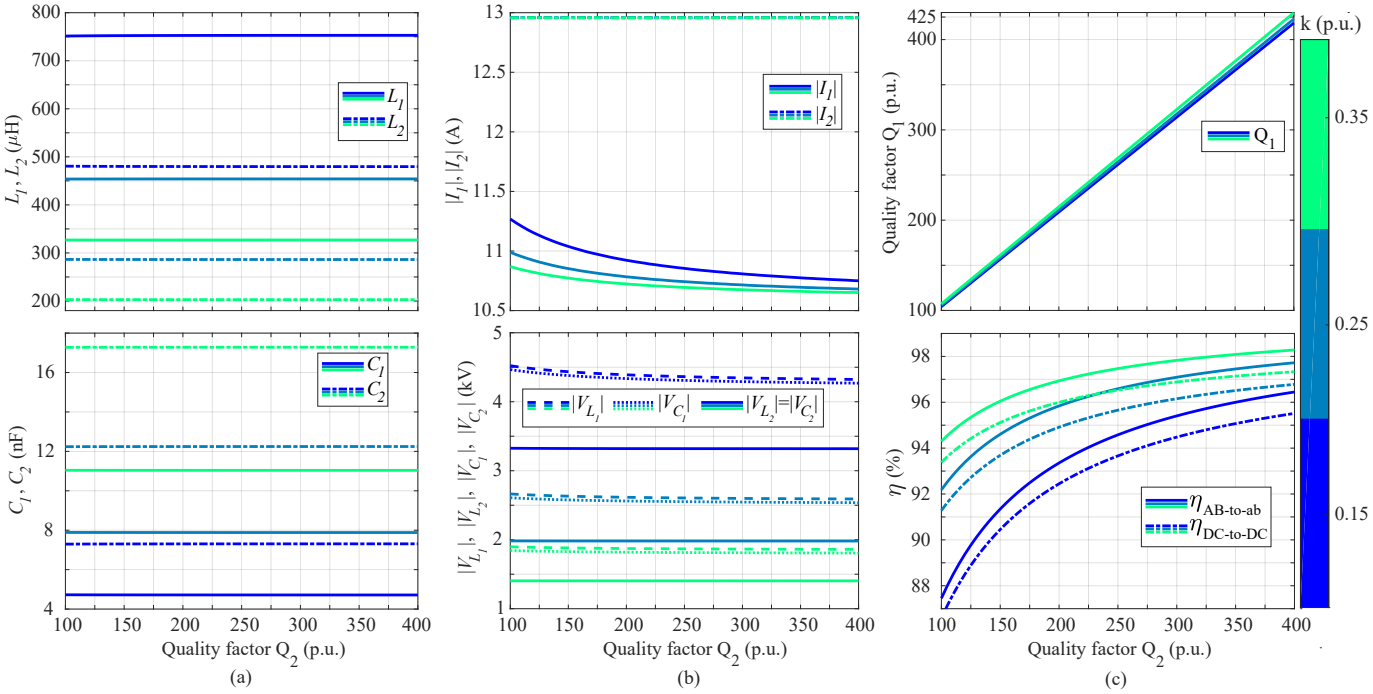

Fig. 3. Parameters of the 3.7 kW IPT system resulting for different coupling k and secondary coil's quality factor Q_2 (M=94.14 μH). (a) Coils' self-inductance L_1 and L_2, and compensation capacitance C_1 and C_2. (b) Peak current and peak voltage in both primary and secondary resonant circuits. (c) Primary coil's quality factor Q_1 from (6) with a=1.02, the resonant circuit's efficiency $\eta_{\text{AB-to-ab}}$ and the overall efficiency $\eta_{\text{DC-to-DC}}$ of the IPT system.

(6). This ensures that the IPT circuit's resonant frequency is within the allowed range from the standard. Moreover, it guarantees that the equivalent resistive load R_L=$\frac{V_{out}}{I_{out}}$ coincides with the optimum load $R_{L,opt}$ achieving the load impedance matching described in [15]–[17]. Additionally, the bifurcation phenomenon defined in [4] is avoided by imposing the condition explained in [11] on the primary and secondary the coils' quality factor Q_1, Q_2.

$$\begin{cases} f_0 = 79...90\,\text{kHz} \\ k\sqrt{L_1 L_2} = \dfrac{8}{\pi^2}\dfrac{V_{in}V_{out}}{\omega_0 P_{out}} \quad \text{from (2) and (5)} \\ R_L = R_{L,opt} = \dfrac{\pi^2}{8}\omega_0 M\sqrt{\dfrac{R_2}{R_1}} \\ Q_1 = \dfrac{2a^2Q_2^2(1-\sqrt{(1-k^2)})-1}{k^2Q_2} \quad \text{where:} \\ a > 1, \quad Q_1 = \dfrac{\omega_0 L_1}{R_1}, \quad Q_2 = \dfrac{\omega_0 L_2}{R_2} \end{cases} \tag{6}$$

A relationship between the coupled coils' parameters can be computed from (6) which depends on Q_1, Q_2 and k. This dependence is going to be discussed in the example of Section III-A. A specific solution of the coupled coils' parameters would result from their physical characteristics which are a consequence of their geometry and structure. This point is addressed in Section III-B.

Finally, C_1 and C_2 can be calculated from (3) by imposing $X_1 > 0$ and X_2=0. This choice translates into an inductive primary current necessary to achieve the zero voltage switching (ZVS) turn-on of the H-bridge inverter [5].

III. Example: Design Methodology for a 3.7 kW EV Wireless Charging System

This section gives an example of the generalized guidelines defined in Section II for the power level of 3.7 kW.

A. Analytical computation

From (5), when considering $P_{out,max}$=3.4 kW, V_{in}=490 V, V_{out}=400 V, and f_0=79 kHz, the target M is estimated to be 94.14 μH. At this point, the optimized combination of inductance and capacitance needs to be selected.

Fig. 3 shows the resulting circuit parameters depending on the values of k, Q_1, and Q_2, which, in turn, result from the coils' dimensions and geometry.

Fig. 3(a) shows that the inductance and the capacitance are independent of Q_1 and Q_2. For instance, to achieve the same M, the required L_1 and L_2 increases as k drops. Therefore, for the same value of k, both Q_1 and Q_2 derive from the coils' resistance.

According to Fig. 3(b), the secondary circuit's current stress $|I_2|$ is invariant of the coils' parameters since V_{out} and P_{out} have been fixed while keeping flexibility on V_{in}. For this reason, the current stress on the primary circuit $|I_1|$ can differ among these designs up to 5.5%. Generally, $|I_1|$ is lower for higher values of k and Q_2. As a consequence of the current stress and the inductance and capacitance values in Fig. 3(a), the voltage stress at both primary and secondary circuits can drop up to 60% as k increases. The resulting voltage stress highly influences the design of the passive components. When considering the main coils, enough distance needs to be allocated between each neighboring turn to ensure isolation. This distance depends on the total voltage stress. On the

TABLE I

DIMENSIONS (mm) VALID FOR BOTH COILS REFERRING TO FIG. 4.

x_a, y_a, z_a	x_f, $x_{f,unit}$, y_f, $y_{f,unit}$, z_f	x_c, y_c	$z_{f\text{-}c}$	$z_{f\text{-}a}$	d
570, 370, 2	559, 43, 364, 28, 4.1	545, 350	2	4	2.5
Ferrite units: E planar core 3C95; Litz wire: 600 strands x 0.071mm					

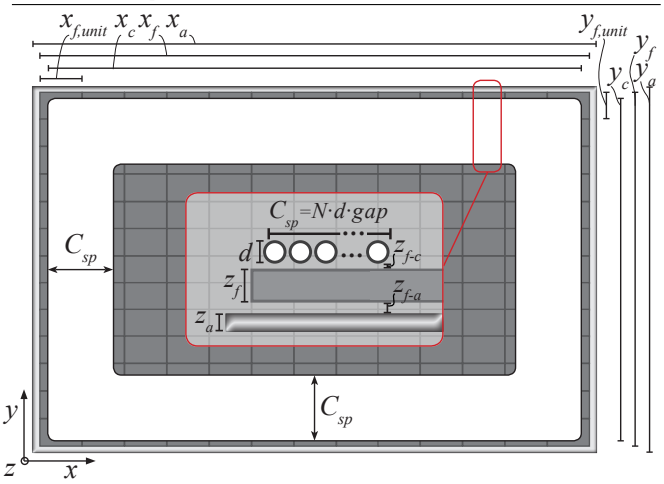

Fig. 4. Coils' geometry which dimensions are specified in Table I.

other hand, the voltage stress on the compensation capacitors influences the required number of series connections of the single unit capacitor based on its voltage rating. A larger number of series connections translate into more necessary parallel connections to reach the same capacitance value. Consequently, this affects the number of used components, the total size of the printed circuit board (PCB), and above all the system total cost.

By using (6), Fig. 3(c) shows that in all designs, the bifurcation phenomenon is avoided if $Q_1 > Q_2$. Moreover, the power transfer efficiency improves with higher k and Q_2 values because of the lower current stress and the reduced coils' resistance. It can be noticed that, to reach a certain DC-to-DC efficiency $\eta_{\text{DC-to-DC}}$ when k is low, there is the need to design coils with higher quality factor than in the case with higher k. For example, to achieve $\eta_{\text{DC-to-DC}}$=95.8%, Q_2=395 is required at k=0.15, while Q_2=235 is required at k=0.25, and Q_2=165 is required at k=0.35. Higher Q_2 values can be obtained by changing the coil's structure or employing a Litz wire with a larger diameter, i.e., reducing the current density of the coil. Some considerations on this matter are discussed in Section III-B.

B. Coils design through FEM analysis

In Section III-A, different options have been explored for the choice of the IPT system parameters, which are summarized in Fig. 3. These are dependent on k and Q_2, which are consequences of the coils' geometry and structure.

In EV applications, the available space for the coils' placement is limited, which restraints their maximum area. In this analysis, the main coils' dimensions were given as listed in Table I referring to Fig. 4. The dimensions of the aluminum shield, the ferrite layer, the outer size of the winding, and the Litz wire's diameter are fixed, and they are identical for both coils. However, there is still room to choose their

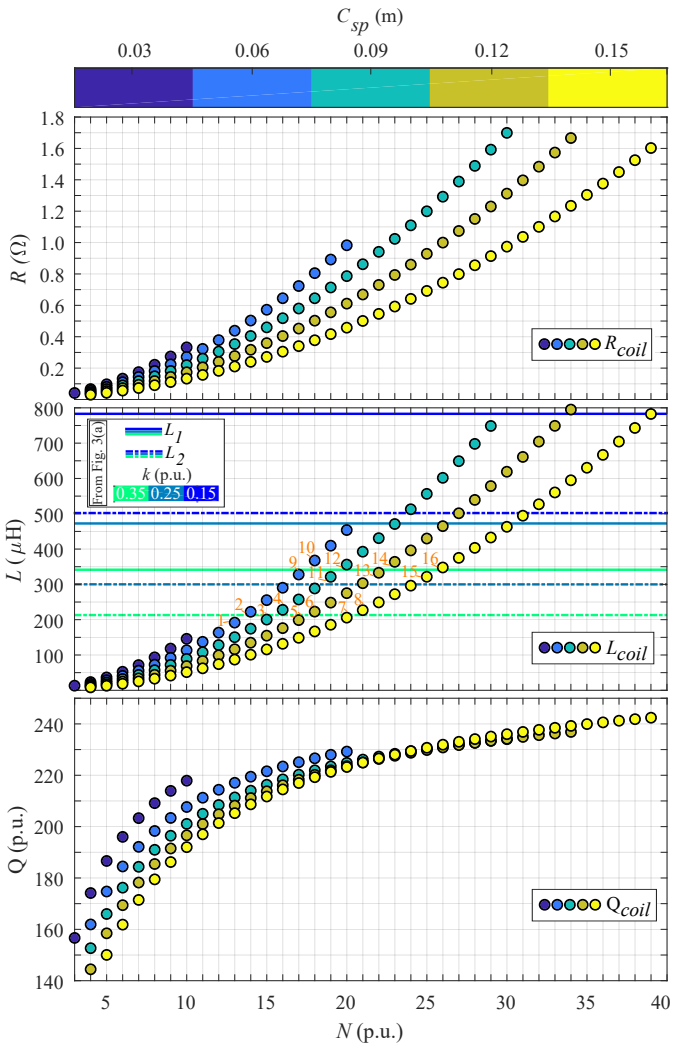

Fig. 5. Parameters of single (uncoupled) coils that have different coil's spread C_{sp} and number of turns N, resulting from the FEM analysis. The coils' geometry is specified in Table I taking as a reference Fig. 4.

coil's spread C_{sp} defined in Fig. 4, their number of turns N and the distance between them in the z-direction, being $Z_{ag} \geq 100\,\text{mm}$. It must be noted that the following method also applies if there are more degrees of freedom in the coils' structure or geometry. Additionally, this approach could be also included in a coils' design based on the multi-objective optimization such as [15], [16] and [18]. In those cases, the spectrum of possible solutions would be wider.

The values of C_{sp1}, C_{sp2}, N_1, N_2 and Z_{ag} are selected by performing a FEM analysis on different possible designs of the coupled coils while making sure that the conditions in (6) are satisfied. According to Section III-A, the coupled coils must result in M=94.14 μH at f_0=79 kHz for the aligned condition. Moreover, the optimum load condition in (6) must satisfy $R_{L,opt}$=R_L=47.06 Ω which translate into $\frac{R_2}{R_1}$=0.666. To avoid the bifurcation phenomenon, $Q_1 > Q_2$ must hold.

1) FEM analysis of single (uncoupled) coils: To understand the influence of C_{sp} and N on the coil's inductance L and resistance R, a sensitivity analysis has been performed by sweeping those parameters. The rectangular coil in Fig. 4 has

(a) (b) (c) (d)

Fig. 6. The coils' implementation for the 3.7 kW EV wireless charging prototype: (a) winding of the primary coil, (b) Winding of the secondary coil, (c) ferrite layer and (d) aluminum shield defined in Fig. 4 which is identical for both coils.

TABLE II

PARAMETERS OF THE COUPLED COILS FROM THE FEM ANALYSIS. THE PRIMARY AND SECONDARY COILS' DESIGNS DERIVE FROM FIG. 5.

Coupled coils from Fig. 5					
Secondary	Primary	k	$\frac{R_2}{R_1}$	Q_1, Q_2(p.u.)	Z_{ag}(mm)
2	12	0.324	0.613	220, 219	105.5
	13	0.333	0.650	219, 220	105.0
	16	0.32	0.627	222, 220	106.5
3	11	0.357	0.643	220, 213	105.5
	15	0.356	0.639	222, 214	109.4
4	10	0.316	0.662	227, 215	108.0
	12	0.320	0.655	222, 217	114.0
	14	0.317	0.638	223, 217	120.0
5	15	0.357	0.643	224, 214	114.5
6	13	0.335	0.687	223, 217	119.5
	16	0.327	0.664	227, 218	122.8
7	11	0.352	0.666	221, 216	110.5
	15	0.352	0.659	224, 218	117.6
8	9	0.332	0.744	225, 216	104.8
	13	0.332	0.693	223, 220	121.5
	16	0.325	0.672	228, 221	125.0

been considered which fixed dimensions are specified in Table I. In this first stage, the coil is placed in the free air, and it is not coupled to another coil to ensure that a specific magnetic coupling does not influence the results.

Fig. 5 shows the resulting coil's resistance R_{coil}, inductance L_{coil}, and quality factor Q_{coil} for different C_{sp} and N. These have been found from the FEM analysis performed through COMSOL Multiphysics. The same outer diameter d=2.5 mm of the Litz wire has been considered for all designs since the coil's current density will not change drastically for the same value of M as shown in Fig. 3(b). Additionally, for each value of C_{sp}, the maximum allowable N is found such that $gap \geq 1.2$, where gap is dimensionless as defined in Fig. 4. This ensures a minimum distance between adjacent turns that guarantees electrical isolation and limits the proximity effect.

According to Fig. 5, it is worth mentioning that a higher value of Q_{coil} can be achieved by reducing C_{sp} for the same N as long as $N \leq$25. On the other hand, a larger C_{sp} can accommodate more number of turns N and, consequently, higher values of self-inductance can be achieved.

In Fig 5, the target coils' self-inductance values L_1 and L_2 found in Fig. 3(a) are compared to L_{coil} resulting from the FEM analysis of different designs. It is possible to notice that C_{sp}=0.03 m results in L_{coil} lower than the target values for $k \leq$0.35. Therefore, that coil's spread is discarded.

The analysis of single coils in Fig. 5 is valuable since it gives a first indication of the parameters to be expected from a certain coil's design. Nevertheless, it is essential to also assess

TABLE III

PARAMETERS OF THE CHOSEN COUPLED COILS DESIGN FROM THE FEM ANALYSIS COMPARED TO THE VALUES RESULTING FROM THE LABORATORY IMPLEMENTATION IN FIG. 6.

	C_{sp}(m), N(p.u.)	Z_{ag}=111 mm		L(μH)	R(Ω)	Q(p.u.)	M(μH)
L_1	0.09, 19		FEM	332.3	0.744	221.6	93.75
L_2	0.15, 20			215.8	0.494	216.6	
Coils in Fig. 5/Table II: primary=11, secondary=7			lab	338.0	0.650	258.1	93.90
				223.7	0.440	252.4	

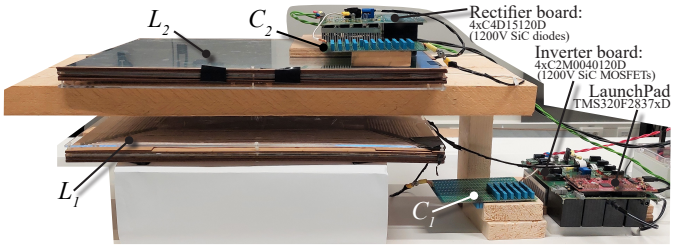

Fig. 7. Laboratory prototype of the 3.7 kW EV wireless charging system.

the final configuration with the coupled coils in which their parameters might differ due to the magnetic coupling.

2) FEM analysis of coupled coils: According to Fig. 3(c), greater values of k at the aligned position lead to higher power transfer efficiency for the same coils' quality factor. Therefore, this analysis first considers the coils' designs in which L_1 and L_2 correspond to the target values at k=0.35. In Fig 5, these are labeled with orange numbers. In particular, the coupled coils' configurations that satisfy $\frac{R_2}{R_1}$=(1±0.04)·0.666 are chosen since most likely to meet the target of $\frac{R_2}{R_1}$=0.666. The distance Z_{ag} between the coils is chosen such that M=94.14 μH. A combination of coupled coils is considered acceptable only if the target M is met while $Z_{ag} \geq 100$ mm.

The combinations of coupled primary and secondary coils are assessed through FEM analysis, and their resulting parameters are summarized in Table II. Among all the coupled coils, the chosen configuration is the one that has 11 as primary coil and 7 as secondary coil because it has the highest k while meeting the requirements on $\frac{R_2}{R_1}$ and Z_{ag}.

The implementation of the chosen coupled coils is shown in Fig. 6(a)-(d). In Table III, the coils' parameters measured at 79 kHz through a LCR meter are compared to the ones resulting from the FEM analysis.

C. Laboratory prototype and experimental results

The overall wireless charging system is shown in Fig. 7 and the parameters are listed in Table IV. One bidirectional DC power supply has been used as power source, while a second one has been employed in current-sinking mode to emulate the EV battery's behavior. When considering the lump

TABLE IV
CIRCUIT PARAMETERS AND COMPONENTS USED IN THE PROPOSED 3.7 kW EV WIRELESS CHARGING SYSTEM IN FIG. 7.

Circuit parameters					**Component**	**Function**	**Units**	**Manufacturer**	**Name**
f (Hz)	79110		**Primary**	**Secondary**	MOSFETs*	Inverter	4	CREE/Wolfspeed	C2M0040120D
$P_{\text{grid,max}}$ (kW)	3.7	L_1, L_2	338.0	224.7	Diodes**	Rectifier	4		C4D15120D
V_{in}(V)	[360 500]	C_1, C_2 (nF)	13.45	18.53	6.8 nF	C_1	8x4	EPCOS	B32671L
V_{batt}(V)	[280 400]	R_{L_1}, R_{L_2} (Ω)	0.65	0.44	500 V_{rms}	C_2	11x4		
$R_{L,opt}$ (Ω)	48.78	M (μH)	[61.72	93.90]	**Misalignment** [(x,y,z) mm]		$M_{\text{max}} \rightarrow (0, 0, Z_{ag})$		
Z_{ag} (mm)	111		[M_{min}	M_{max}]			$M_{\text{min}} \rightarrow [(90, 0, Z_{ag})]$		
*[$R_{ds,on}$=50 mΩ, E_{off}=15 μJ]; **[V_F=0.8 V, r=75 mΩ]									
Measuring and supplying equipment	Oscilloscope: YOKOGAWA DLM4058 2.5GS/s 500MHz Power analyzer: YOKOGAWA WT500 Bidirectional DC power supplies: DELTA ELEKTRONIKA SM500-CP-90 (input), SM1500-CP-30 (output)								

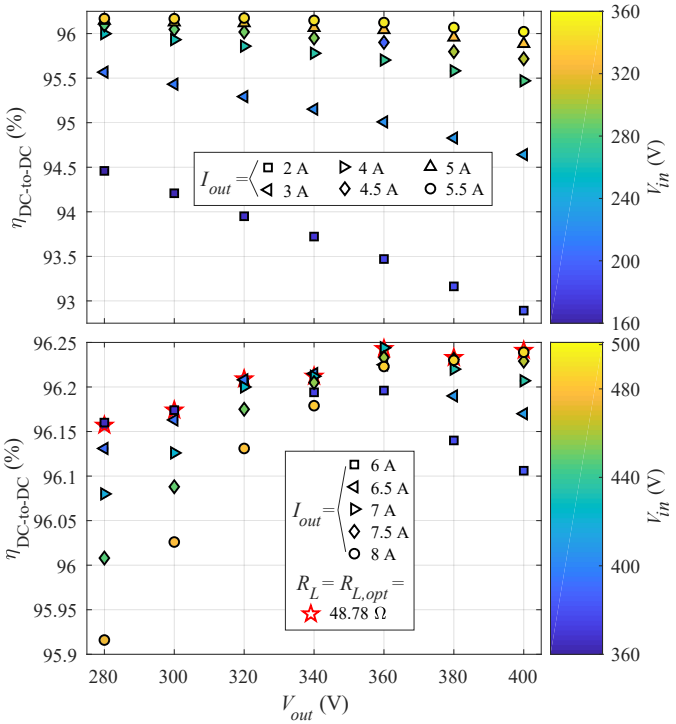

Fig. 8. Measured $\eta_{\text{DC-to-DC}}$ at different load conditions while M=M_{max}. The output current I_{out} has been regulated by controlling V_{in}.

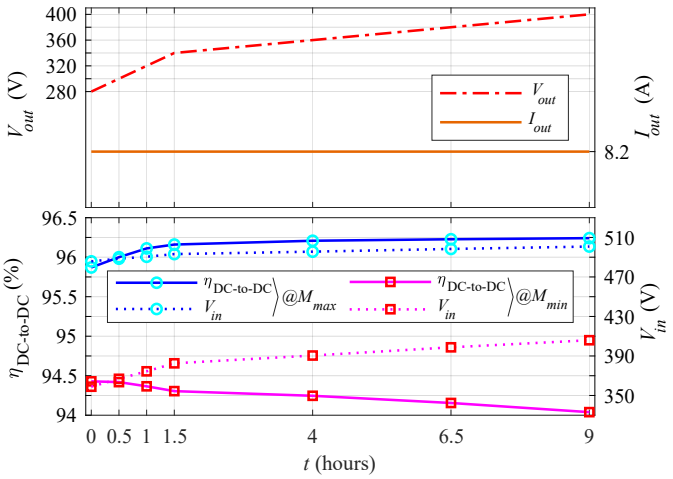

Fig. 9. Measured $\eta_{\text{DC-to-DC}}$ and supplied V_{in} at both M=M_{max} and M=M_{min} for the CC mode of a typical EV battery charging cycle. In this example, the total energy received by the battery would be about 26.5 kW h.

resistance of the coils, the compensation capacitors, and the semiconductor devices, the equivalent optimum load results in $R_{L,opt}$=48.78 Ω which is acceptable since it translates into a nominal P_{out}=3.28 kW $\leq$ $P_{out,max}$=3.4 kW. Two points of coils' alignment have been considered of which mutual inductance corresponds to M=M_{max} and M=M_{min}.

At M=M_{max}, the DC-to-DC efficiency $\eta_{\text{DC-to-DC}}$ has been measured at different output voltage and current values to characterize the overall IPT system. These values are shown in Fig. 8. Thereby, I_{out} has been regulated by controlling V_{in} through the input DC power supply. This could be performed through a boost-like PFC converter for the operating points with I_{out} $\geq$ 6 A since the required V_{in} is in the range 360...500 V. Lower I_{out} could be set by phase shifting the H-bridge inverter in Fig. 1 to reduce the fundamental component of V_{AB}. According to Fig. 8, the highest $\eta_{\text{DC-to-DC}}$ can be achieved throughout the entire V_{out} range by operating at the optimum load condition, i.e., when R_L=$R_{L,opt}$.

In Fig. 9, the measured $\eta_{\text{DC-to-DC}}$ at both M=M_{max} and M=M_{min} are plotted for the constant-current (CC) charging profile where I_{out}=8.2 A. Only the CC charging mode is considered because it takes place for most of the charging process in EV applications with the WPT1 power class. Additionally, the measured waveforms at the nominal battery voltage are shown in Fig. 10 for both coils' alignments. It must be noted that the ZVS turn-on of the H-bridge inverter is always maintained with the chosen compensation capacitance.

According to Fig. 9, it is possible to follow the CC charging profile for the entire battery voltage range by regulating V_{in} through the PFC stage at both coils' alignments. The misalignment range can be further extended by phase-shifting the H-bridge inverter in Fig. 1. When the coils' misalignment occurs, the efficiency drops up to 2.2% at the nominal battery voltage. This efficiency drop has three main causes. First, according to (5), a lower V_{in} is required to achieve the same output power. Consequently, as shown in Fig. 10(b), there is a higher current circulating at the primary circuit, which increases the conduction losses. Second, as described in (6), the optimum load $R_{L,opt}$ is directly proportional to M. This means that $R_{L,opt}$ differs for the two coils' alignments: $R_{L,opt}$=48.78 Ω for M=M_{max}, and $R_{L,opt}$=32.98 Ω M=M_{min}. However, independently of M, the equivalent resistive load R_L varies in the range 34.14...48.78 Ω during the CC charging mode. This means that, at M=M_{min}, R_L never matches $R_{L,opt}$. Due to this characteristic of $R_{L,opt}$, the highest efficiency is reached at the minimum battery voltage when M=M_{min}. Finally, Fig. 10 shows that the primary current is more inductive M=M_{min}

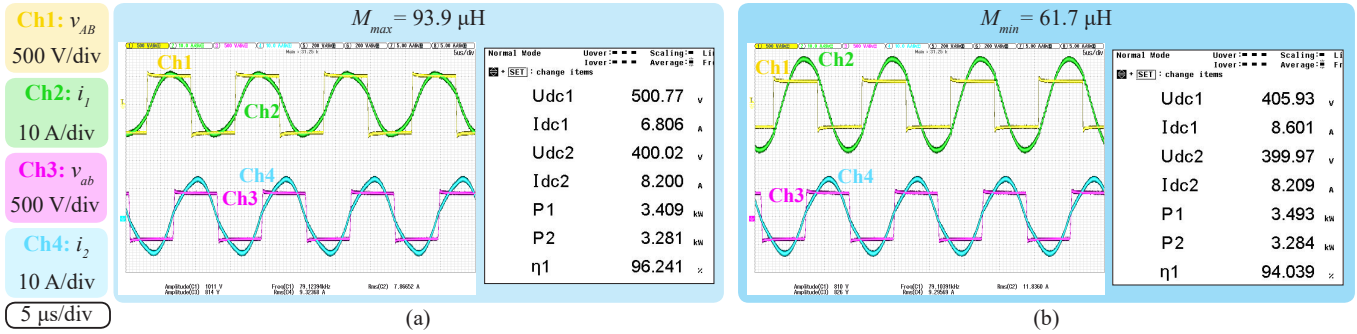

Fig. 10. Measured circuit waveforms and DC-to-DC efficiency at: (a) M=M_{max}, and (b) M=M_{min}.

than in the aligned case which worsens the turn-off losses. The reason for this becomes clear by analyzing the expression of the input impedance Z_{in} in (7), which has been derived from (1) assuming that X_1 >0 and X_2=0 at $\omega = \omega_0$. Considering the variations of X_1 negligible, it can be noticed from (7) that R_{in}, i.e., the real part of Z_{in}, is directly dependent on M^2. This means that, as M decreases due to the coils' misalignment, R_{in} would also decrease leading to a more inductive Z_{in}.

$$Z_{in} = \frac{\boldsymbol{V}_{AB}}{\boldsymbol{I}_1} = \underbrace{R_1 + \frac{(\omega_0 M)^2}{R_2 + R_{ac}}}_{R_{in}} + j \underbrace{\left(\omega_0 L_1 - \frac{1}{\omega_0 C_1}\right)}_{X_{in}=X_1} \quad (7)$$

IV. Conclusion

This paper explains how to select the coupled coils' inductance and compensation capacitance in S-S compensated EV wireless charging systems. This selection starts with identifying the input design specifications, such as the target output power, operating frequency, and the available DC input and output voltage ranges. These input specifications result in a target value of the coupled coils' mutual inductance. The coils' coupling and quality factor have been found to influence the overall efficiency for the same mutual inductance value. Those parameters depend on the coils' structure. To understand how the coil's structure influences these parameters, a sensitivity analysis has been performed through the finite element method considering the power level of 3.7 kW. Coupled coils' combinations which differ in number of turns, coil's spread and air gap have been analyzed, preferring the pairs with the highest magnetic coupling. The most suitable design has been implemented, achieving 96.24% as peak DC-to-DC efficiency at full power, i.e., 3.28 kW. The DC input voltage is controlled to achieve the constant current charging profile and to deliver the same output power when the coils are misaligned. When the mutual inductance drops of 44% with respect to the aligned case, the measured efficiency drops 2.2% at full power.

References

[1] Z. Zhang, H. Pang, A. Georgiadis, and C. Cecati, "Wireless power transfer—an overview," *IEEE Transactions on Industrial Electronics*, vol. 66, pp. 1044 – 1058, 2019.

[2] S. Li and C. C. Mi, "Wireless power transfer for electric vehicle applications," *IEEE Journal of Emerging and Selected Topics in Power Electronics*, vol. 3, pp. 4 – 17, 2015.

[3] C.-S. Wang, G. Covic, and O. Stielau, "General stability criterions for zero phase angle controlled loosely coupled inductive power transfer systems," in *27th Annual Conference of the IEEE Industrial Electronics Society (IECON)*, 2001.

[4] ——, "Power transfer capability and bifurcation phenomena of loosely coupled inductive power transfer systems," *IEEE Transactions on Industrial Electronics*, vol. 51, no. 1, pp. 148–157, 2004.

[5] S. Li, W. Li, J. Deng, T. D. Nguyen, Chunting, and C. Mi, "A double-sided lcc compensation network and its tuning method for wireless power transfer," *IEEE Transactions on Vehicular Technology*, vol. 64, pp. 2261 – 2273, 2015.

[6] W. Li, H. Zhao, J. Deng, S. Li, and C. C. Mi, "Comparison study on ss and double-sided lcc compensation topologies for ev/phev wireless chargers," *IEEE Transactions on Vehicular Technology*, vol. 65, no. 6, pp. 4429–4439, 2016.

[7] Y. Chen, H. Zhang, C.-S. Shin, C.-H. Jo, S.-J. Park, and D.-H. Kim, "An efficiency optimization-based asymmetric tuning method of double-sided ¡italic¿lcc¡/italic¿ compensated wpt system for electric vehicles," *IEEE Transactions on Power Electronics*, vol. 35, no. 11, pp. 11 475–11 487, 2020.

[8] C.-S. Wang, O. Stielau, and G. Covic, "Design considerations for a contactless electric vehicle battery charger," *IEEE Transactions on Industrial Electronics*, vol. 52, no. 5, pp. 1308–1314, 2005.

[9] S. Chopra and P. Bauer, "Analysis and design considerations for a contactless power transfer system," in *IEEE 33rd International Telecommunications Energy Conference (INTELEC)*, 2011.

[10] W. Zhang and C. C. Mi, "Compensation topologies of high-power wireless power transfer systems," *IEEE Transactions on Vehicular Technology*, vol. 65, no. 6, pp. 4768–4778, 2016.

[11] F. Grazian, W. Shi, T. B. Soeiro, J. Dong, P. van Duijsen, and P. Bauer, "Quality factor based design guideline for optimized inductive power transfer," in *2020 IEEE PELS Workshop on Emerging Technologies: Wireless Power Transfer (WoW)*, 2020, pp. 178–183.

[12] R. Steigerwald, "A comparison of half-bridge resonant converter topologies," *IEEE Transactions on Power Electronics*, vol. 3, pp.

[13] F. Grazian, W. Shi, J. Dong, P. van Duijsen, T. B. Soeiro, and P. Bauer, "Survey on standards and regulations for wireless charging of electric vehicles," in *AEIT International Conference of Electrical and Electronic Technologies for Automotive (AEIT AUTOMOTIVE)*, 2019.

[14] *J2954 (R) Wireless Power Transfer for Light-Duty Plug-In/ Electric Vehicles and Alignment Methodology*, SAE International Std., Oct. 2020.

[15] R. Bosshard, J. W. Kolar, J. Mühlethaler, I. Stevanovic, B. Wunsch, and F. Canales, "Modeling and η-α-pareto optimization of inductive power transfer coils for electric vehicles," *IEEE Journal of Emerging and Selected Topics in Power Electronics*, vol. 3, pp. 50 – 64, 2015.

[16] S. Bandyopadhyay, P. Venugopal, J. Dong, and P. Bauer, "Comparison of magnetic couplers for ipt-based ev charging using multi-objective optimization," *IEEE Transactions on Vehicular Technology*, vol. 68, no. 6, pp. 5416–5429, 2019.

[17] F. Grazian, W. Shi, T. B. Soeiro, J. Dong, and P. Bauer, "Electric vehicle charging based on inductive power transfer employing variable compensation capacitance for optimum load matching," in *IECON 2020 The 46th Annual Conference of the IEEE Industrial Electronics Society*, 2020, pp. 5262–5267.

[18] W. Shi, J. Dong, T. B. Soeiro, C. Riekerk, F. Grazian, G. Yu, and P. Bauer, "Design of a highly efficient 20-kw inductive power transfer system with improved misalignment performance," *IEEE Transactions on Transportation Electrification*, vol. 8, no. 2, pp. 2384–2399, 2022.